Received: 14 April 2024 | Revised: 20 May 2024 | Accepted: 22 May 2024

IET Renewable Power Generation

DOI: 10.1049/rpg2.13021

The Institution of Engineering and Technology WILEY

ORIGINAL RESEARCH

Low-carbon demand response program for power systems considering uncertainty based on the data-driven distributionally robust chance constrained optimization

Ruifeng Zhao[1] | **Zehao Song**[2] | **Yinliang Xu**[2] | **Jiangang Lu**[1] | **Wenxin Guo**[1] | **Haobin Li**[1]

[1]Electric Power Dispatch Center, Guangdong Power Grid Corporation, Guangzhou, People's Republic of China

[2]Tsinghua-Berkeley Shenzhen Institute (TBSI), Tsinghua Shenzhen International Graduate School, Tsinghua University, Shenzhen, People's Republic of China

Correspondence
Zehao Song, Tsinghua-Berkeley Shenzhen Institute (TBSI), Tsinghua Shenzhen International Graduate School, Tsinghua University, Shenzhen, People's Republic of China.
Email: songzh22@mails.tsinghua.edu.cn

Funding information
China Southern Power Grid Corporation Limited Project "Energy Management and Cluster Control Technology for Active Distribution Networks", Grant/Award Number: GDKJXM20222144

Abstract

The demand response (DR) program is an effective solution to promote the low-carbon operation of power systems with increasing penetration of renewable energy sources (RESs). This paper proposes a low-carbon DR program for power systems to enhance both the environmental friendliness and uncertainty resilience of the system operation. The system operator aims to minimize both the system's operation cost and carbon trading cost. To handle the uncertainty associated with stochastic RES generation power and load consumption power, a data-driven method named the two-sided distributionally robust chance-constrained (TS-DRCC) approach is adopted to enhance the system's uncertainty resilience. A ladder-type carbon trading scheme is utilized to calculate the carbon emission cost of the system. Comprehensive analyses of case studies have been conducted to validate that the proposed strategy can effectively reduce the total carbon emissions and total operation costs with good uncertainty resilience performance. The proposed low-carbon DR program is verified to achieve 63.64% more carbon emission reduction compared with the conventional DR program. Besides this, the proposed low-carbon DR program can also achieve 4.39% carbon-intensive generation power reduction and 5.52% RES power consumption compared with the conventional DR program.

1 | INTRODUCTION

1.1 | Background

Worldwide global warming and climate change problems call for an urgent need to replace carbon-intensive and high-pollution fossil energy sources with low-carbon and clean renewable energy sources (RESs) in power systems [1, 2] In recent years, the installed capacity of renewable energy generators such as wind turbines (WTs) and photovoltaic arrays (PVs) around the world has continued to grow [3, 4]. However, due to the significant impact of unpredictable weather factors on the output of renewable energy sources such as wind and solar energy, RESs exhibit strong randomness and uncertainty [5]. The integration of large-scale RESs poses a great challenge to the safe and stable operation of power systems, and the traditional passive operation mode [6] is no longer suitable for power systems with high penetration RESs. An effective solution to improve the system operation flexibility is to guide distributed energy resources (DERs) on the demand side, such as flexible loads (FLs) to cooperate with the operation of the power systems [7]. In this context, the demand response (DR) program has been proposed to fully exploit the flexibility potential of FLs for enhancing the system operation flexibility in the face of large-scale RES penetration [8].

Ruifeng Zhao and Zehao Song contributed equally to this work.

1.2 | Literature review

1.2.1 | DR program

The DR program has received increasing attention due to its efficiency in unlocking the flexibility potential of the demand side [9, 10]. Generally, the DR program can be divided into two categories including price-based DR programs and incentive-based DR programs [11]. In [12], a power system optimal dispatch model considering the residential users' participation uncertainty and response uncertainty is proposed by using incentive-based DR programs. However, the network operation constraints are ignored in [12] and thus the proposed model may not ensure the system operation security in practical power system operation. A supply-demand cooperative responding strategy based on both day-ahead and intra-day time scales is proposed in [13] by incorporating both price-based DR programs and incentive-based DR programs. Yet the uncertainty of RES power forecast error is assumed to follow the Gaussian distribution in [13], which may not correspond with the real situation and lead to relatively high decision errors. An economic dispatching strategy considering the uncertainties of RES power and DR programs is proposed in [14] based on both price-based DR programs and incentive-based DR programs. The information gap decision theory (IGDT) is adopted to evaluate risks associated with uncertainties in [14].

1.2.2 | Uncertainty problem

Properly coping with uncertainty associated with the demand-side DERs (including stochastic RESs and user loads) is crucial to improving the RES accommodation to the new power systems [15]. To address the uncertainty problem, various approaches have been developed to enhance the resilience of the system operation strategy under the stochastic environment. The representative approaches for handling uncertainty are the stochastic optimization (SO) method, chance-constrained (CC) method, and robust optimization (RO) method.

The SO method [16] is typically quite intuitive because it considers the stochastic scenarios of uncertainties. Therefore, the effectiveness of the SO method heavily depends on the forecast data accuracy. However, the forecast errors are inevitable because of the inherent volatile and stochastic nature of the demand-side DERs. One possible way to mitigate the negative influence caused by inaccurate forecast data is to enlarge the stochastic scenarios set. However, this will inevitably lead to heavy computational burden and complexity. In [17], the DR program for multi-energy industrial microgrids is formulated as a scenario-based SO problem to tackle the uncertainty of PV power. Similar to [17], a scenario-based SO model is proposed in [18] to solve the energy and flexibility dispatch problem of a microgrid with solar and stationary battery systems. Inspired by the model predictive control (MPC) method [19], which is quite efficient in coping with real-time uncertainty, the formulated SO problem in [18] is solved in the rolling horizon by considering the newest forecast profiles for PV power and demand-side load power.

The CC method [20] assumes the uncertainties follow certain known probability distributions and allows violation of uncertain constraints with pre-defined probability. The CC method can achieve better computational efficiency compared with the SO method. However, as the same with the SO method, the effectiveness of the CC method also relies on accurate probability distribution, which is hard to get in practical applications. A CC-based electric vehicle (EV) optimal dispatching strategy considering EV drivers' response uncertainty is proposed in [21]. The conditional value at risk (CVaR) approximation method and the sequential convex approximation (SCA) method are adopted to make the chance constraints tractable. In [22], a CC-based economic dispatch (ED) model for power systems is proposed to co-optimize the generation problem of the conventional distributed generators (DGs) and curtailment strategies of RESs.

Different from the SO method and the CC method mentioned above, the RO method [23] does not need any pre-known information about the uncertainties, it considers the worst scenario within the ambiguity set to ensure the robustness. In [24], an optimal DR program based on the distribution locational marginal price (DLMP) is proposed, and the uncertain PV power generation is tackled by the RO method. A two-stage RO method based on the adaptive uncertainty set is proposed in [25] to solve the ED problem of the microgrid by utilizing EV resources. However, the RO method often derives the over-conservative strategy since it only considers the worst scenario, which is typically a low-probability scenario in practical application.

Fortunately, some data-driven methods like the distributionally robust optimization (DRO) [26] approach can offer a promising way to better cope with the uncertainty problem. The data-driven DRO approach only needs historical data about the uncertainty rather than prior knowledge about the actual uncertainty distribution. By properly processing the historical data (i.e. the training data) about the uncertainty, the DRO approach can gain knowledge from the hidden information about the training data set to assist the decision procedure. The main differences between the DRO approach and the aforementioned methods can be summarized as follows: (i) Unlike the SO/CC method which relies on the uncertainty distribution forecast accuracy, the DRO method does not rely on the assumed exact uncertainty distribution. Instead, the DRO method establishes the ambiguity set of the unknown uncertainty distribution, in this way, the DRO method can still retain its robustness under the worst uncertainty distribution case; (ii) Compared with the RO method, the DRO method can further utilize the hidden information of the uncertainty data set to avoid the over-conservative decision.

In [27], a Wasserstein metric (WM) based DRO model is proposed to co-optimize the transactive energy trading and network operation of interconnected microgrids. However, the impact of the uncertainty on the network operation constraints hasn't been investigated in [27]. The distributionally

robust chance-constrained (DRCC) method [28] has been proposed to better handle the uncertain operation constraints more efficiently. The DRCC method can ensure that the violation probability of the uncertain constraints can be limited within the preferred range regardless of the probability distribution of the uncertainty, which is a good characteristic in the face of inaccurate forecast data. To address the uncertainties of RESs and unpredictable contingencies, a comprehensive DRCC-based framework for microgrids is proposed in [29]. Yet [29] considers the one-sided DRCC (OS-DRCC) operation constraints, which will lead to the inexact constraint approximation problem under the stochastic environment.

1.2.3 | Decarbonization problem

The decarbonization of power systems has been regarded as an indispensable element of the power system transition process. In [30], the carbon capture unit is utilized to capture the carbon emission of the carbon-intensive generators to implement the low-carbon ED of the combined heat and power virtual power plants (VPPs). Yet the utilization of the carbon capture unit will add more equipment investment costs. A fixed carbon trading price mechanism is adopted in [31] to consider the carbon emission cost during the system operation. However, the fixed carbon trading price may not be suitable for further promoting the power system's low-carbon operation since it can not properly distinguish the carbon emission responsibilities among different entities. To overcome this shortcoming of the fixed carbon trading price mechanism, the ladder-type carbon trading price scheme [32] is adapted to further motivate participants to reduce their carbon emissions. More recently, a new concept named the committed carbon emission operation region (CCEOR) has been proposed in [33] to efficiently analyze the low carbon operation of integrated energy systems (IESs). The proposed CCEOR in [33] can visually characterize the low-carbon feasible space and provide comprehensive low-carbon operation information of operation conditions for the IESs.

1.3 | Contributions

Inspired by the aforementioned problems and inspiring works, a low-carbon DR program for power systems considering uncertainty is proposed in this paper. The main contributions of this paper are listed as follows.

- Different from the existing works [12, 13] only focusing on the electricity DR program, this paper also takes the carbon emission impact of the system's strategies into consideration and further proposes a low-carbon DR program.
- Compared with the OS-DRCC approach in [29, 34] to handle the uncertainty constraints, this paper adopts a more accurate two-sided DRCC (TS-DRCC) approach to enhance the uncertainty resilience of the system strategies under the stochastic real-world environment.
- The impact of the uncertainty on the power system's operation constraints has been comprehensively considered in this work compared with [27] to provide better decision guidance for the system operator.

1.4 | Organisation

The rest of the paper is organized as follows. Section 2 illustrates the proposed low-carbon DR program framework in detail. Section 3 presents the problem formulation process of the proposed low-carbon DR program for power systems by using the TS-DRCC approach to cope with the uncertainty problem. To make the origin problem tractable, Section 4 provides the second-order cone (SOC) based convex reformulation method to convexify the origin intractable implicit distributionally robust chance constraints. Comprehensive case studies are provided in Section 5 to verify the advantages of the proposed strategy. Finally, the conclusions are presented in Section 6.

2 | DATA-DRIVEN LOW-CARBON DR PROGRAM FRAMEWORK

The framework of the proposed low-carbon DR program for power systems considering uncertainty is presented in Figure 1. First, the uncertainty historical data set can be pre-processed by calculating the first-order and second-order moment information. Then, the ambiguity set based on the limited moment information about the uncertainty can be formulated regardless of the concrete uncertainty distribution. The uncertainty constraints are formulated as distributionally robust chance constraints first. To make the intractable and implicit distributionally robust chance constraints tractable and explicit ones, the SOC-based convex reformulation method is adopted to convexify and approximate these constraints. Finally, by considering the carbon emission impact of the system's operation strategies based on the ladder-type carbon trading scheme, the low-carbon DR program of the power systems is implemented.

3 | PROBLEM FORMULATION

3.1 | Ambiguity set formulation

To cope with the uncertainty problem during the system operation horizon, the moment-based DRCC approach is adopted in this paper. The ambiguity set defined by first-order and second-order moment information is built to restrict the underlying possible probability distributions of RES power forecast errors, which is given as follows:

$$\mathcal{P}_t^{\mathrm{R}} := \{\mathbb{P}_{\xi_t^{\mathrm{R}}} : \mathbb{E}_{\mathbb{P}}[\boldsymbol{\xi}_t^{\mathrm{R}}] = \boldsymbol{\mu}_t^{\mathrm{R}}, \mathbb{E}_{\mathbb{P}}[(\boldsymbol{\xi}_t^{\mathrm{R}} - \boldsymbol{\mu}_t^{\mathrm{R}})(\boldsymbol{\xi}_t^{\mathrm{R}} - \boldsymbol{\mu}_t^{\mathrm{R}})^{\top}] = \boldsymbol{\Sigma}_t^{\mathrm{R}}\}, \tag{1}$$

where $\mathbb{E}_{\mathbb{P}}$ denotes the expectation operator and $\boldsymbol{\xi}_t^{\mathrm{R}}$ is the node RES power forecast error at time slot t, $\boldsymbol{\mu}_t^{\mathrm{R}}$ and $\boldsymbol{\Sigma}_t^{\mathrm{R}}$ are mean

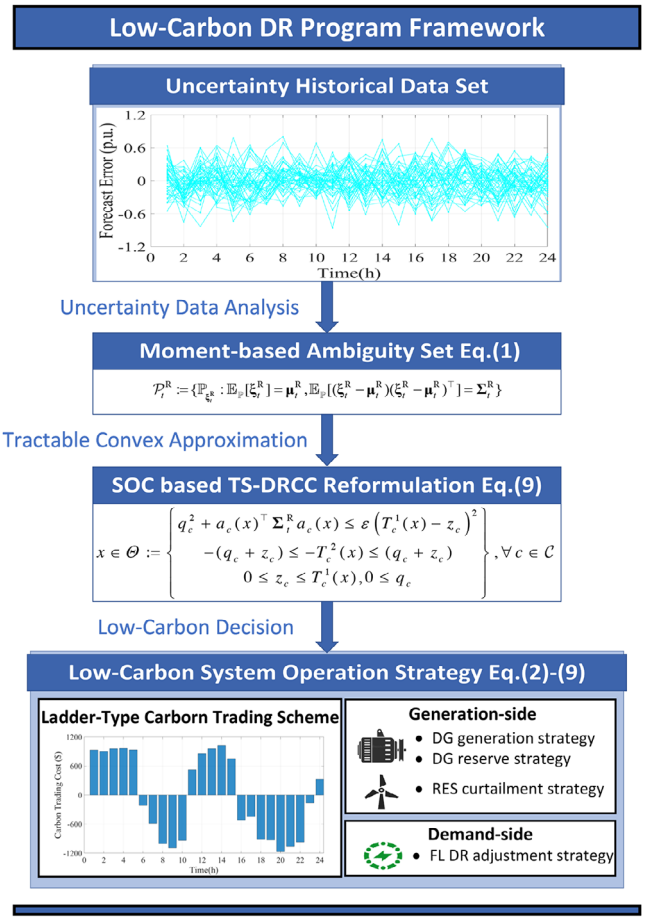

FIGURE 1 The framework of the proposed low-carbon DR program.

value vector and covariance matrix of $\boldsymbol{\xi}_t^{\mathrm{R}}$, respectively. The ambiguity set formulation process for the load power forecast error is provided in Appendices, Section A for the clarity of this paper.

3.2 | Objective function

Based on the moment-based DRCC approach, the operation cost minimization problem of the system considering uncertainty is formulated as follows:

$$f^{\mathrm{Sys}} = \sum_{t\in\mathcal{T}} \left(f_t^{\mathrm{G}} + f_t^{\mathrm{R}} + f_t^{\mathrm{L}} + f_t^{\mathrm{C}}\right), \tag{2a}$$

$$f_t^{\mathrm{G}} = \underbrace{\mathbf{P}_t^{\mathrm{G}\top}\mathbf{C}_2^{\mathrm{G}}\mathbf{P}_t^{\mathrm{G}} + \mathbf{C}_1^{\mathrm{G}\top}\mathbf{P}_t^{\mathrm{G}}}_{\text{DG generation cost}} + \underbrace{\mathbf{C}^{\mathrm{R}\top}(\mathbf{R}_t^{\mathrm{U,G}} + \mathbf{R}_t^{\mathrm{D,G}})}_{\text{DG reserve cost}}, \tag{2b}$$

$$f_t^{\mathrm{R}} = \underbrace{\mathbf{C}^{\mathrm{R,cut}\top}\mathbf{P}_t^{\mathrm{R,cut}}}_{\text{RES curtailment cost}}, \tag{2c}$$

$$f_t^{\mathrm{L}} = \underbrace{\mathbf{C}^{\mathrm{L,dis}\top}\Delta\mathbf{P}_t^{\mathrm{L}}}_{\text{Load discomfort cost}}, \tag{2d}$$

$$f_t^{\mathrm{C}} = \underbrace{\begin{cases} -\pi_t^{\mathrm{C}}(2+3\lambda)\delta + \pi_t^{\mathrm{C}}(1+3\lambda)\left(E_t^{\mathrm{Sys,tr}} + 2\delta\right), E_t^{\mathrm{Sys,tr}} \le -2\delta \\ -\pi_t^{\mathrm{C}}(1+\lambda)\delta + \pi_t^{\mathrm{C}}(1+2\lambda)\left(E_t^{\mathrm{Sys,tr}} + \delta\right), -2\delta < E_t^{\mathrm{Sys,tr}} \le -\delta \\ \pi_t^{\mathrm{C}}(1+\lambda)E_t^{\mathrm{Sys,tr}}, -\delta < E_t^{\mathrm{Sys,tr}} \le 0 \\ \pi_t^{\mathrm{C}}E_t^{\mathrm{Sys,tr}}, 0 < E_t^{\mathrm{Sys,tr}} \le \delta \\ \pi_t^{\mathrm{C}}\delta + \pi_t^{\mathrm{C}}(1+\rho)\left(E_t^{\mathrm{Sys,tr}} - \delta\right), \delta < E_t^{\mathrm{Sys,tr}} \le 2\delta \\ \pi_t^{\mathrm{C}}(2+\rho)\delta + \pi_t^{\mathrm{C}}(1+2\rho)\left(E_t^{\mathrm{Sys,tr}} - 2\delta\right), 2\delta < E_t^{\mathrm{Sys,tr}} \le 3\delta \\ \pi_t^{\mathrm{C}}(3+\rho)\delta + \pi_t^{\mathrm{C}}(1+3\rho)\left(E_t^{\mathrm{Sys,tr}} - 3\delta\right), 3\delta < E_t^{\mathrm{Sys,tr}} \end{cases}}_{\text{Carbon emission cost}}. \tag{2e}$$

In (2), (2a) is the total system operation cost. (2b) is the operation cost of the DGs at time slot t, which includes the generation cost and the reserve cost. (2c) and (2d) are the RES curtailment and load DR adjustment cost at time slot t, respectively. (2e) is the carbon trading cost at time slot t.

3.3 | Constraints

3.3.1 | DG operation constraints

The operation constraints of the DGs are formulated as follows:

$$\mathbf{R}_t^{\mathrm{G}} = \mathbf{d}_t^{\mathrm{G}}\left(\mathbf{e}^{\top}\boldsymbol{\xi}_t^{\mathrm{R}}\right), \tag{3a}$$

$$\underline{\mathbf{P}}^{\mathrm{DG}} \le \mathbf{P}_t^{\mathrm{G}} \le \overline{\mathbf{P}}^{\mathrm{DG}}, \tag{3b}$$

$$\mathbf{0}_{N^{\mathrm{B}}\times 1} \le \mathbf{R}_t^{\mathrm{U,G}} \le \bar{\mathbf{R}}^{\mathrm{U,G}}, \tag{3c}$$

$$\mathbf{0}_{N^{\mathrm{B}}\times 1} \le \mathbf{R}_t^{\mathrm{D,G}} \le \bar{\mathbf{R}}^{\mathrm{D,G}}, \tag{3d}$$

$$\mathbf{P}_t^{\mathrm{G}} + \mathbf{R}_t^{\mathrm{U,G}} - \left(\mathbf{P}_{t-1}^{\mathrm{G}} - \mathbf{R}_{t-1}^{\mathrm{D,G}}\right) \le \bar{\mathbf{r}}^{\mathrm{U,G}}, \tag{3e}$$

$$\mathbf{P}_{t-1}^{\mathrm{G}} + \mathbf{R}_{t-1}^{\mathrm{U,G}} - \left(\mathbf{P}_t^{\mathrm{G}} - \mathbf{R}_t^{\mathrm{D,G}}\right) \le \bar{\mathbf{r}}^{\mathrm{D,G}}, \tag{3f}$$

$$\mathbf{0}_{N^{\mathrm{B}}\times 1} \le \mathbf{d}_t^{\mathrm{G}}, \mathbf{1}_{1\times N^{\mathrm{G}}} \cdot \mathbf{d}_t^{\mathrm{G}} = 1. \tag{3g}$$

In (3), (3a) is the re-dispatch constraint of the DGs at time slot t. (3b) is the generation power constraint of the DGs at time slot t. (3c) and (3d) are upward and downward reserve power constraints of the DGs at time slot t, respectively. (3e) and (3f) are upward and downward ramping power constraints of the DGs at time slot t, respectively. (3g) is the re-dispatch coefficient constraint of the DGs at time slot t. Note that During the practical system operation period, the actual generation power and redispatch power of DGs at the last time period is known in the current time period. Thus, the ramping constraints of DGs (3e) and (3f) can be formulated as deterministic constraints. As for (3c) and (3d), the reserve power constraints of DGs can be further formulated as the DRCC operation constraints since the reserve power should be scheduled before the practical system operation day. The planned reserve power

should satisfy the ramping limits of the DGs with the system's desired confidence level.

3.3.2 | RES operation constraints

The operation constraints of the RESs are formulated as follows:

$$\mathbf{0}_{N^{\mathrm{B}}\times 1} \le \mathbf{P}_t^{\mathrm{R,cut}} \le \mathbf{P}_t^{\mathrm{R,fore}}. \tag{4}$$

(4) is the curtailment power constraint of the RESs at time slot t.

3.3.3 | DR operation constraints

The operation constraints of the FLs are formulated as follows:

$$\mathbf{P}_t^{\mathrm{FL}} = \Delta\mathbf{P}_t^{\mathrm{L}} + \mathbf{P}_t^{\mathrm{L,fore}}, \tag{5a}$$

$$\Delta\underline{\mathbf{P}}_t^{\mathrm{L}} \le \Delta\mathbf{P}_t^{\mathrm{L}} \le \Delta\overline{\mathbf{P}}_t^{\mathrm{L}}, \tag{5b}$$

$$\sum_{t\in\mathcal{T}} \Delta\mathbf{P}_t^{\mathrm{L}} = \mathbf{0}_{N^{\mathrm{B}}\times 1}, \tag{5c}$$

$$\sum_{t\in\mathcal{T}} \left| \frac{\Delta\mathbf{P}_t^{\mathrm{L}}\cdot\Delta t}{\mathbf{P}_t^{\mathrm{L,fore}}\cdot\Delta t} \right| \le \overline{\mathbf{U}}^{\mathrm{L,dis}}. \tag{5d}$$

In (5), (5a) is the adjusted load power constraint of the FLs at time slot t. (5b) is the DR adjustment power limit constraint of the FLs at time slot t. (5c) can ensure that the total energy demand of the FLs can still be satisfied after the load power adjustment. (5d) is the load power adjustment discomfort tolerance constraint of the FLs.

3.3.4 | Carbon trading constraints

The ladder-type carbon trading scheme [35] is considered in this paper to further promote the low-carbon operation of the system. The system's carbon trading constraints are formulated as follows:

$$E_t^{\mathrm{Sys,init}} = \delta_t^{\mathrm{Sys,init}} \sum_{i\in\mathcal{N}^{\mathcal{B}}} P_{t,i}^{\mathrm{L,fore}}, \tag{6a}$$

$$E_t^{\mathrm{Sys,ac}} = \sum_{i\in\mathcal{N}^{\mathcal{B}}} e_i^{\mathrm{G}} P_{t,i}^{\mathrm{G}}, \tag{6b}$$

$$E_t^{\mathrm{Sys,tr}} = E_t^{\mathrm{Sys,init}} - E_t^{\mathrm{Sys,ac}}. \tag{6c}$$

In (6), (6a) is the initial free carbon emission quota constraint of the system at time slot t. (6b) is the actual carbon emission constraint of the system at time slot t. (6c) is the carbon trading constraint of the system at time slot t.

3.3.5 | Network operation constraints

The system's network operation constraints are formulated as follows:

$$\mathbf{P}_t^{\mathrm{inj}} = \mathbf{SF}^{\mathrm{G}}\left(\mathbf{P}_t^{\mathrm{G}} + \mathbf{R}_t^{\mathrm{G}}\right) + \mathbf{SF}^{\mathrm{R}}\left(\mathbf{P}_t^{\mathrm{R,fore}} - \mathbf{P}_t^{\mathrm{R,cut}} + \boldsymbol{\xi}_t^{\mathrm{R}}\right) - \mathbf{SF}^{\mathrm{L}}\mathbf{P}_t^{\mathrm{FL}}, \tag{7a}$$

$$\mathbf{P}_t^{\mathrm{line}} = \mathbf{A}\cdot\mathbf{P}_t^{\mathrm{inj}}, \tag{7b}$$

$$\mathbf{1}_{1\times N^{\mathrm{B}}}\cdot\mathbf{P}_t^{\mathrm{inj}} = 0. \tag{7c}$$

In (7), (7a) is the node injection power constraint of the system at time slot t. (7b) is the branch power constraint of the system at time slot t. (7c) is the system power balance constraint at time slot t.

3.3.6 | DRCC operation constraints

Considering the impact of the uncertainty on the system's operation constraints. The system's DRCC operation constraints are formulated as follows:

$$\inf_{\mathbb{P}_{\boldsymbol{\xi}_t^{\mathrm{R}}}\in\mathcal{P}_t^{\mathrm{R}}} \mathbb{P}_{\boldsymbol{\xi}_t^{\mathrm{R}}}\left\{ \underline{\mathbf{P}}^{\mathrm{line}} \le \mathbf{A}\cdot\mathbf{P}_t^{\mathrm{inj}} \le \overline{\mathbf{P}}^{\mathrm{line}} \right\} \ge 1-\varepsilon_{\mathrm{line}}, \tag{8a}$$

$$\inf_{\mathbb{P}_{\boldsymbol{\xi}_t^{\mathrm{R}}}\in\mathcal{P}_t^{\mathrm{R}}} \mathbb{P}_{\boldsymbol{\xi}_t^{\mathrm{R}}}\left\{ -\mathbf{R}_t^{\mathrm{D,G}} \le \mathbf{d}_t^{\mathrm{G}}\left(\mathbf{e}^{\top}\boldsymbol{\xi}_t^{\mathrm{R}}\right) \le \mathbf{R}_t^{\mathrm{U,G}} \right\} \ge 1-\varepsilon_{\mathrm{G,R}}, \tag{8b}$$

$$\inf_{\mathbb{P}_{\boldsymbol{\xi}_t^{\mathrm{R}}}\in\mathcal{P}_t^{\mathrm{R}}} \mathbb{P}_{\boldsymbol{\xi}_t^{\mathrm{R}}}\left\{ \underline{\mathbf{P}}^{\mathrm{G}} \le \mathbf{P}_t^{\mathrm{G}} + \mathbf{d}_t^{\mathrm{G}}\left(\mathbf{e}^{\top}\boldsymbol{\xi}_t^{\mathrm{R}}\right) \le \overline{\mathbf{P}}^{\mathrm{G}} \right\} \ge 1-\varepsilon_{\mathrm{G,P}}. \tag{8c}$$

In (8), (8a) is the DRCC branch power limit constraint of the system at time slot t and $\varepsilon_{\mathrm{line}}$ is the system risk preference parameter for the branch power constraint. (8b) is the DRCC reserve power constraint of the DGs at time slot t and $\varepsilon_{\mathrm{G,R}}$ is the system risk preference parameter for the reserve power constraint of the DGs. (8c) is the DRCC re-dispatch power constraint of the DGs at time slot t and $\varepsilon_{\mathrm{G,P}}$ is the system risk preference parameter for the re-dispatch power constraint of the DGs. Note that the system risk preference parameters $\varepsilon_{\mathrm{line}}, \varepsilon_{\mathrm{G,R}}, \varepsilon_{\mathrm{G,P}}$ represent the desired confidence level (i.e. the allowable constraint violation probability) of the corresponding DRCC system operation constraints (8a)–(8c), respectively. (8b) means that the reserve power of the DGs should be able to compensate for the power deviation caused by the uncertainties at time slot t with the confidence level of $1-\varepsilon_{\mathrm{G,R}}$. (8c) means that the re-dispatch power of the DGs should be limited within the generation power range at time slot t with the confidence level of $1-\varepsilon_{\mathrm{G,P}}$.

4 | CONVEX REFORMULATION FOR THE DRCC OPERATION CONSTRAINTS

The origin DRCC operation constraints (8a)–(8c) are intractable and implicit, which will bring great challenges to the system's decision process. To make the origin problem solvable, the DRCC operation constraints (8a)-(8c) can be reformulated into convex constraints by using the SOC-based convex reformulation technique in [36] as follows:

$$\inf_{\mathbb{P}_{\xi_t^{\mathrm{R}}}\in\mathcal{P}_t^{\mathrm{R}}} \mathbb{P}_{\xi_t^{\mathrm{R}}}[l_c(x) \leqslant a_c(x)^{\top}\boldsymbol{\xi}_t^{\mathrm{R}} + b_c(x) \leqslant u_c(x)] \geqslant 1-\varepsilon_c, \forall c \in \mathcal{C}, \tag{9a}$$

$$T_c^1(x) = \frac{u_c(x) - l_c(x)}{2}, T_c^2(x) = \frac{u_c(x) + l_c(x)}{2}, \forall c \in \mathcal{C}, \tag{9b}$$

$$\inf_{\mathbb{P}_{\xi_t^{\mathrm{R}}}\in\mathcal{P}_t^{\mathrm{R}}} \mathbb{P}_{\xi_t^{\mathrm{R}}}[-T_c^1(x) \leqslant a_c(x)^{\top}\boldsymbol{\xi}_t^{\mathrm{R}} + b_c(x) - T_c^2(x) \leqslant T_c^1(x)] \geqslant 1-\varepsilon_c, \forall c \in \mathcal{C}, \tag{9c}$$

$$x \in \Theta_c := \left\{ \begin{array}{c} q_c^2 + a_c(x)^{\top}\boldsymbol{\Sigma}_t^{\mathrm{R}} a_c(x) \leqslant \varepsilon\left(T_c^1(x) - z_c\right)^2 \\ -(q_c + z_c) \leqslant -T_c^2(x) \leqslant (q_c + z_c) \\ 0 \leqslant z_c \leqslant T_c^1(x), 0 \leqslant q_c \end{array} \right\}, \forall c \in \mathcal{C}. \tag{9d}$$

In (9), (9a) is the compact form of the DRCC operation constraints (8a)-(8c). $l_c(x)$ and $u_c(x)$ are the affine mappings of the lower bound and upper bound of the decision variable x for the *cth* DRCC operation constraint at time slot t, respectively. $a_c(x)$ and $b_c(x)$ are the affine mappings of the decision variable x for the *cth* DRCC operation constraint at time slot t, respectively. With the introduction of $T_c^1(x)$ and $T_c^1(x)$ as defined in (9b), (9a) can be rewritten into a symmetric form as shown in (9c). Finally, the SOC-based convex reformulation constraints of (9a) are shown in (9d).

5 | CASE STUDIES

5.1 | Simulation setup

Experimental simulations are conducted to verify the advantages and effectiveness of the proposed low-carbon DR program. All the simulations are conducted on a 64-bit Windows environment laptop with Intel(R) Core(TM) i5-12500H 3.10 GHz CPU and 16 GB RAM. The models are coded in MATLAB 2021b with the YALMIP toolbox and solved by the Gurobi 10.0 solver. The topology and parameter data information of the IEEE 9-Bus and 39-Bus systems is provided in [37].

5.2 | IEEE 9-Bus system

We conduct numerical tests on the IEEE 9-Bus system in this case study. The topology of the IEEE 9-Bus system is shown in Figure 2. The system base capacity is 100 MVA. The system has 3 DGs, 3 RES generators, and 3 FLs located at 3 different nodes. Other network parameters and DG generation cost coefficients are the same as those of the standard IEEE 9-Bus system. The reserve cost coefficients are set as 5 times the DG generation generation cost linear term coefficients. The daily load demand forecast power and RES generation forecast power curves are shown in Figure 3. The RES curtailment cost and DR adjustment cost coefficients are set as 500 $/ MWh and 50 $/ MWh, respectively. The carbon trading price and carbon trading quantity are set as 70 $/ ton and 2 ton, respectively. The carbon trading reward/penalty price coefficients are set as 0.25/0.2, respectively. The system's initial carbon emission quota coefficient and DG carbon emission factor are set as 0.3 ton/MWh and 0.85 ton/MWh, respectively. The maximum DR adjustment power is set as 40% of the load forecast power. The node load maximum discomfort tolerance is set as 20%. All the system risk preference parameters are set as 0.3 for the simulations except for the sensitivity analysis of the risk preference parameters. The system operation horizon and operation time interval are set as 24 h and 1 h, respectively.

5.2.1 | Ambiguity set setting

We adopt the Monte Carlo simulation approach to generate 10000 scenarios of RES power forecast error following the multivariate Gaussian distribution $\mathcal{N}(\boldsymbol{\mu}_t^{\mathbf{R}}, \boldsymbol{\Sigma}_t^{\mathbf{R}})$. The parameter settings of $\mathcal{N}(\boldsymbol{\mu}_t^{\mathbf{R}}, \boldsymbol{\Sigma}_t^{\mathbf{R}})$ are shown as follows:

$$\left\{ \begin{array}{l} \boldsymbol{\Sigma}_t^{\mathrm{R}}(i,i) = \zeta \cdot \mathbf{P}_t^{\mathrm{R,fore}}(i) \\ \boldsymbol{\Sigma}_t^{\mathrm{R}}(i,j) = \rho_{i,j} \cdot \zeta \cdot \mathbf{P}_t^{\mathrm{R,fore}}(i) \cdot \mathbf{P}_t^{\mathrm{R,fore}}(j) \end{array} \right., \tag{10}$$

where ζ and $\rho_{i,j}$ are the ambiguity parameters to control the uncertainty level. $\boldsymbol{\Sigma}_t^{\mathrm{R}}(i,i)$ denotes the *ith* row *ith* column element of $\boldsymbol{\Sigma}_t^{\mathrm{R}}$ and $\mathbf{P}_t^{\mathrm{R,fore}}(i)$ denotes the *ith* row element of $\mathbf{P}_t^{\mathrm{R,fore}}$.

Note that we set $\boldsymbol{\mu}_t^{\mathbf{R}} = \mathbf{0}_{N^{\mathrm{B}}\times 1}$, $\zeta = 0.05$, and $\rho_{i,j} = 0.2$ in all the simulations for the RES uncertainty ambiguity. We randomly select 500 samples from the generated 10000 scenarios to form the training data. The rest of them form the test data set to simulate the stochastic real-world environment. The consideration for the load uncertainty ambiguity is similar to the RES uncertainty ambiguity mentioned above. The detailed process is shown in Appendices, Section A.

5.2.2 | Case studies setting

We compare comprehensive case studies with other system operation modes to verify the advantages and effectiveness of the low-carbon DR program considering uncertainty. The setup for cases are listed as follows:

- *Case I*: The traditional system operation mode without DR program.

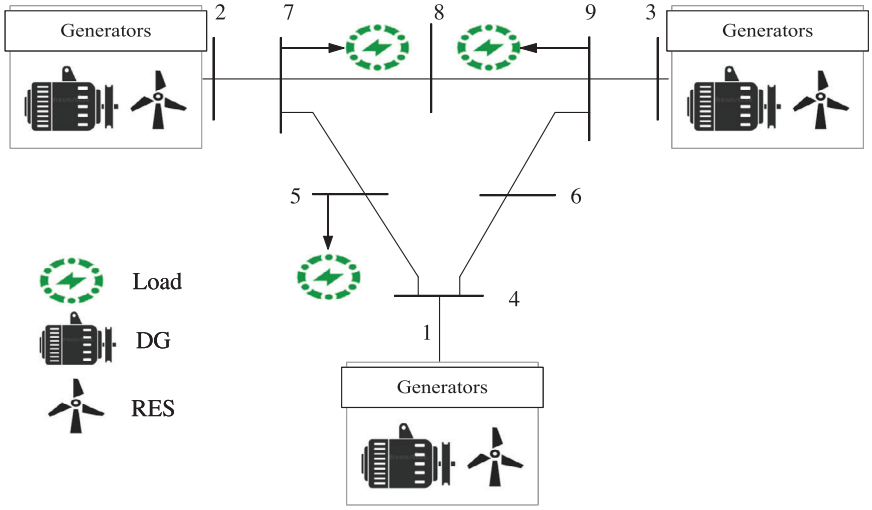

FIGURE 2 Topology of the IEEE 9-Bus system.

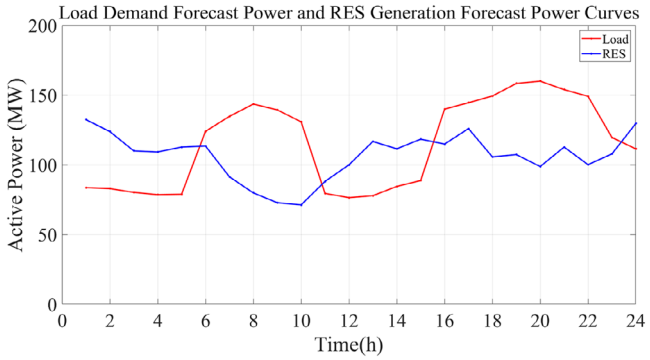

FIGURE 3 Load demand forecast power and RES generation forecast power curves.

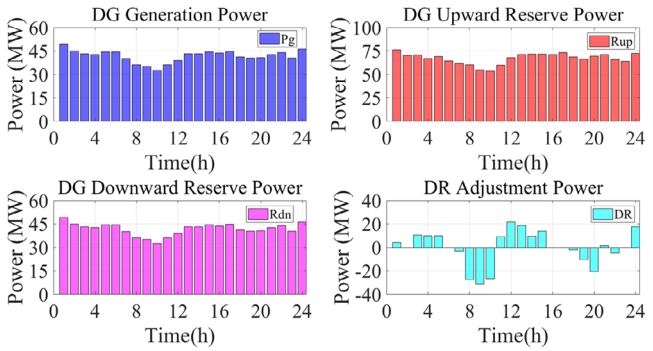

FIGURE 4 DG generation power, upward and downward reserve power, and load DR adjustment power profiles of Case III.

- *Case II*: The electricity DR program without carbon emission impact concern.
- *Case III*: The proposed low-carbon DR program using the TS-DRCC approach as in [36].
- *Case IV*: The proposed low-carbon DR program using the OS-DRCC approach as in [34].

5.2.3 | Simulation results and analysis

The DG operation strategies (including the DG generation power, upward and downward power denoted as Pg, Rup, and Rdn, respectively.) and load DR adjustment strategies (the load DR adjustment power denoted as DR is the increased load power minuses the decreased load power) under Case III are shown in Figure 4. The comparison of the system's power utilization in the IEEE 9-Bus system under Cases I–IV is presented in Table 1. Moreover, the comparison of the system's DR adjustment and RES curtailment strategies is shown in Figure 5. Here we want to emphasize rationality when choosing the system risk preference parameters. Note that in Figure 5 we set $\varepsilon_{\text{line}}, \varepsilon_{\text{G,R}}, \varepsilon_{\text{G,P}}$ as 0.3 for the rational risk parameter case and 0.9999 for the over-optimistic risk parameter case, respectively.

TABLE 1 Comparison of the system's aggregated power utilization during the operation horizon in the IEEE 9-Bus system.

Power item (10^3MW)	Case I	Case II	Case III	Case IV
DG generation power	1.1610	1.0499	1.0038	0.9922
DG upward reserve power	1.3606	1.4004	1.6139	0.9811
DG downward reserve power	1.0710	1.0499	1.0038	0.9922
RES curtailment power	0.9455	0.8345	0.7884	0.7768
DR adjustment power	0.0000	0.2221	0.2545	0.2607

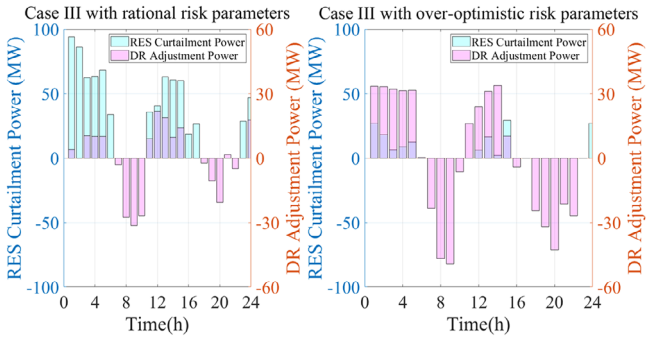

FIGURE 5 RES curtailment power and DR adjustment power of Case III under rational and over-optimistic risk preference parameters.

TABLE 2 Comparison of the system's aggregated operation costs during the operation horizon in the IEEE 9-Bus system.

Cost item (10^4\$)	Case I	Case II	Case III	Case IV
System operation cost	8.1073	6.8388	6.5239	5.3347
DG generation cost	1.2871	1.0955	1.0325	0.9893
DG reserve cost	3.9566	4.0004	4.2599	3.2338
RES curtailment cost	1.4183	1.2517	1.1825	1.1652
DR adjustment cost	0.0000	0.0333	0.0382	0.0391
Carbon trading cost	1.4453	0.4579	0.0108	−0.0926

In Figure 5, we can find that the over-optimistic case nearly reduces the RES curtailment power to zero. This is because by choosing the system risk preference parameters close to 1, the system operator nearly neglects the system operation constraints and utilizes the DR adjustment power to reduce RES curtailment power. However, this kind of over-optimistic operation mode will significantly threaten the system operation security, the system operation constraints violation probability under the test data set is 40.00%. On the contrary, the rational risk parameter case can appropriately improve reasonable RES power consumption while ensuring the system operation security (The violation probability under the rational risk parameter case is 32.20% lower than that of the over-optimistic risk parameter case). Thus, it can be concluded that properly considering the impact of uncertainty on the system operation constraints is of great importance.

It can be concluded from the results in Table 1 that the proposed low-carbon DR program in Case III outperforms Case I and Case II from the aspects of carbon-intensive DG generation power reduction and clean RES power consumption. Case II achieves 9.57% DG generation power reduction and 11.74% RES curtailment power reduction, and Case III achieves 13.54% DG generation power reduction and 16.62% RES curtailment power reduction compared with Case I, respectively. Particularly, Case III achieves 14.59% more DR adjustment power utilization than Case II. Thus, it can be verified that the proposed low-carbon DR program can motivate demand-side DERs to participate in the low-carbon operation of the power systems by considering the carbon emission impact of the DR program on the system operation.

As for Case IV, though it seems to outperform Case III in the aspects mentioned above, it will face greater system operation risk than Case III in practical applications, which will be discussed later.

The comparison of the system's operation costs in the IEEE 9-Bus system under Cases I–IV is presented in Table 2. Note that the system can sell its surplus carbon emission quota at some operation time slots to reduce the carbon trading cost by adjusting the system power utilization profile.

From Table 2, we can find that Case III achieves the lowest costs from the aspects listed in Table 2 except for the DG reserve cost item among Cases I–III. Specifically, Case II achieves 15.65% system operation cost reduction and 14.89% DG generation cost reduction, and Case III achieves 19.53% system operation cost reduction and 19.78% DG generation cost reduction compared with Case I, respectively. Since Case III aims to utilize more clean RES power to promote the low-carbon operation of the system, its DG reserve cost is 7.67% higher than that of Case I to accommodate more fluctuated RES power. However, the results demonstrate that this strategy can eventually reduce the system operation cost and the carbon trading cost. Case IV achieves the best performance at the cost of sacrificing the system's uncertainty resilience, which will be discussed later.

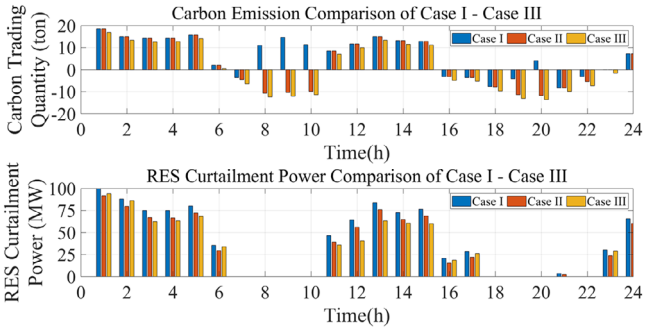

FIGURE 6 Carbon emission and RES curtailment profiles of Cases I–III.

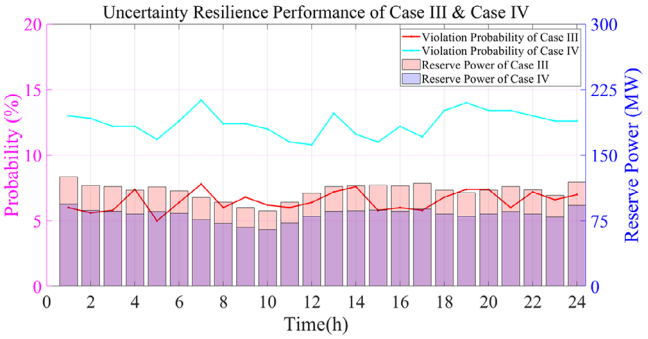

FIGURE 7 Uncertainty resilience performance comparison of Cases III and IV under test data.

The comparison of the system's carbon trading quantity profiles and RES curtailment power profiles of Cases I–III is shown in Fig 6.

It can be concluded from Fig 6 that Case III can reduce the system's carbon trading quantity (i.e. the system's carbon emission quantity) by reducing the RES curtailment power during the system operation horizon. Case III achieves 63.64% carbon emission reduction compared with Case II.

The comparison of the system's uncertainty resilience performance in the IEEE 9-Bus system of Case III and Case IV under the test data set is presented in Figure 7. Note that the violation probability item in Figure 7 refers to the joint constraints violation probability of (8a)–(8c), that is, the system's operation constraints are regarded as being violated as long as there is at least one of the constraint in (8) is violated.

From Figure 7, we can find that the reserve power of Case III is higher than that of Case IV during the system operation horizon. This is because the TS-DRCC approach is more

TABLE 3 Comparison of the system's aggregated operation costs in the IEEE 9-Bus system during the operation horizon under different carbon trading prices.

Cost item(10^4\$) \ π_t^C(\$/ton)	20	40	60	80	100
System operation cost	6.4722	6.5084	6.5313	6.5245	6.5239
Carbon trading cost	0.0605	0.0540	0.0441	-0.0020	-0.0356

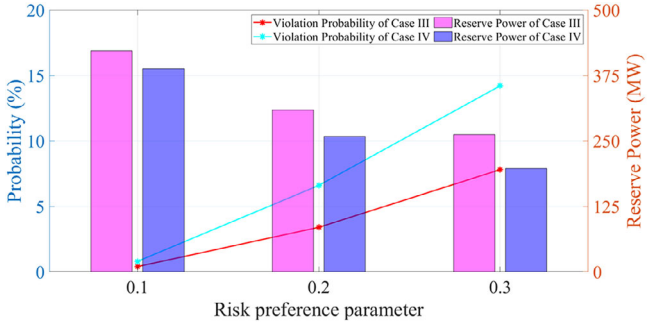

FIGURE 8 Uncertainty resilience performance comparison of Case III and Case IV under test data set with different risk preference parameters.

accurate than the OS-DRCC approach from the aspect of the DRCC constraint convex reformulation process. Therefore, the operation constraints violation probability of Case III is significantly lower than that of Case IV during the system operation horizon, which is crucial to ensure the operation security of the system with high-penetration uncertain RES power integration.

5.2.4 | Sensitivity analysis

The carbon trading price can be regarded as the weighting factor of the system's environmental concern compared with the system's economic concern. The comparison of the system's operation costs and carbon trading costs in the IEEE 9-Bus system under different carbon trading prices is shown in Table 3. It can be found that the most significant system carbon trading cost reduction occurs when the carbon trading price changes from 60\$/ ton to 80\$/ ton. Thus, the reasonable pricing range of the carbon trading price may be within around 60\$/ ton to 80\$/ ton, which is consistent with that of the current carbon market like European carbon trading market [38].

The uncertainty resilience performance comparison of Case III and Case IV under test data set with different risk preference parameters is shown in Figure 8.

It can be found that Case III can achieve a more significant system operation risk reduction compared with Case IV as the risk preference parameter grows, which can further demonstrate the advantages of the adopted TS-DRCC-based approach from the aspect of the strategies' uncertainty resilience.

The comparison of the system's aggregated operation costs in the IEEE 9-Bus system during the operation horizon under different DR adjustment capabilities is shown in Table 4. We can get the conclusion that the system's DG generation cost, RES curtailment cost, and carbon trading cost can be significantly reduced by increasing the maximum DR adjustment power and node load maximum discomfort tolerance parameter. Moreover, the system can achieve considerable operation cost reduction with slightly increased DR adjustment cost. Therefore, the system can improve its operation flexibility to achieve better operation performance by increasing the DR adjustment power within the rational discomfort tolerance range of user loads.

TABLE 4 Comparison of the system's aggregated operation costs in the IEEE 9-Bus system during the operation horizon under different DR adjustment capabilities.

Cost item (10^4\$) \ ($\overline{\Delta P}_t^L / P_t^{L,fore}, \overline{U}^{L,dis}$)	(0.05,0.1)	(0.1,0.2)	(0.2,0.4)
System operation cost	7.1269	6.5604	6.5239
DG generation cost	1.1194	1.0376	1.0325
RES curtailment cost	1.2694	1.1890	1.1825
DR adjustment cost	0.0208	0.0369	0.0382
Carbon trading cost	0.5617	0.0559	0.0108

The comparison of the system's operation strategies in the IEEE 9-Bus system during the operation horizon under different ambiguity set parameters is shown in Table 5. Particularly, we investigate the impact of the diagonal correlation coefficient ζ and the off-diagonal correlation coefficient $\rho_{i,j}$ on the uncertainty level of the formulated ambiguity set. The upward and downward reserve power of DGs can be regarded as the criteria for the uncertainty level. We can find that the impact of the diagonal correlation coefficient on the uncertainty level of the formulated ambiguity set is more significant than that of the off-diagonal correlation coefficient. By comparing the system's operation strategies under ($\rho_{i,j} = 0.2, \zeta = 0.1$), ($\rho_{i,j} = 0.2, \zeta = 0.05$) and ($\rho_{i,j} = 0.4, \zeta = 0.05$), we can see that by enlarging the diagonal correlation coefficient and the off-diagonal correlation coefficient at the same scale, the uncertainty level of the formulated ambiguity set increases more significant by enlarging the diagonal correlation coefficient. Moreover, by comparing the system's operation strategies under ($\rho_{i,j} = 0, \zeta = 0.05$), ($\rho_{i,j} = 0.2, \zeta = 0.05$) and ($\rho_{i,j} = 0.4, \zeta = 0.05$), we can find that the uncertainty level of the formulated ambiguity set doesn't increase significantly as the off-diagonal correlation coefficient increases.

5.3 | IEEE 39-Bus system

We further conduct experimental simulations on the IEEE 39-Bus system to demonstrate the scalability and advantages of the proposed low-carbon DR program. The base capacity of the IEEE 39-Bus distribution system is 100 MVA. The system has 10 DGs, 10 RES generators, and 21 FLs located at 21 different nodes.

The comparisons of the system's power utilization and operation costs in the IEEE 39-Bus system under Cases I–III are

TABLE 5 Comparison of the system's aggregated power utilization during the operation horizon in the IEEE 9-Bus system under different ambiguity set parameters.

Power item (10^3 MW) \ $(\rho_{i,j}, \zeta)$	(0,0.05)	(0.2,0.1)	(0.2,0.05)	(0.4,0.05)
DG generation power	1.0527	1.5074	1.0038	1.2803
DG upward reserve power	1.1296	2.0054	1.6139	1.6029
DG downward reserve power	0.9143	1.4895	1.0038	1.2228
RES curtailment power	0.8373	1.2919	0.7884	1.0648

TABLE 6 Comparison of the system's aggregated power utilization during the operation horizon in the IEEE 39-Bus system.

Power item (10^3MW)	Case I	Case II	Case III
DG generation power	1.9756	1.8241	1.7752
DG upward reserve power	2.5619	2.6499	2.9579
DG downward reserve power	1.8723	1.8241	1.7752
RES curtailment power	1.6309	1.4794	1.4305
DR adjustment power	0.0000	0.3030	0.3367

TABLE 7 Comparison of the system's aggregated operation costs during the operation horizon in the IEEE 39-Bus system.

Cost item ($10^5$$)	Case I	Case II	Case III
System operation cost	1.9119	1.7292	1.6984
DG generation cost	0.0757	0.0687	0.0665
DG reserve cost	0.6651	0.6711	0.7100
RES curtailment cost	0.8155	0.7397	0.7153
DR adjustment cost	0.0000	0.0318	0.0354
Carbon trading cost	0.3555	0.2179	0.1713

presented in Tables 6 and 7, respectively. From the system's power utilization aspect, Case II achieves 7.67% DG generation power reduction and 9.29% RES curtailment power reduction, and Case III achieves 10.14% DG generation power reduction and 12.29% RES curtailment power reduction compared with Case I, respectively. Particularly, Case III achieves 11.12% more DR adjustment power utilization than Case II. From the system's operation costs aspect, Case II achieves 9.56% system operation cost reduction and 9.25% DG generation cost reduction, and Case III achieves 11.17% system operation cost reduction and 12.15% DG generation cost reduction compared with Case I, respectively.

The experimental results of the IEEE 39-Bus system can verify the advantages and the scalability of the proposed method.

6 | CONCLUSIONS

By considering the carbon emission impact of the system's operation strategies, a low-carbon DR program is proposed to better balance the environmental and financial aspects of the power systems while ensuring system operation security at the preferred confidence level. The TS-DRCC approach is adopted to better handle the uncertainty constraints with more accurate convex approximation. To further promote the low-carbon operation of the system, the ladder-type carbon trading scheme is used to differentiate the carbon emission costs associated with various carbon emission quantity intervals. We can get the conclusions according to the experimental simulations as follows. The proposed low-carbon DR program is verified to achieve 63.64% more carbon emission reduction compared with the conventional DR program. Besides this, the proposed low-carbon DR program can also achieve 4.39% carbon-intensive generation power reduction and 5.52% RES power consumption compared with the conventional DR program.

- Incorporating the carbon emission impact of the system's operation strategies can further reduce the system's RES power curtailment and carbon emission. Moreover, the proposed low-carbon DR program can promote the participation of the demand side in the coordinated system operation.
- With the more accurate SOC-based approximation technique, the adopted TS-DRCC approach can achieve better uncertainty resilience performance during the system operation compared with the inexact OS-DRCC approach.
- Modelling the uncertain system operation constraints can reflect the impact of the uncertainty on the system-level and equipment-level operation constraints like the power flow constraints and DG operation constraints, which can further enhance the system operation security as the new power system transition proceeds.

Some parts of this work can be further improved. First, only the FLs are considered in this work to participate in the low-carbon DR program. Besides, the ambiguity sets describing the uncertainties associated with the uncertainties of RESs and loads are based on fixed moment information. In future work, more kinds of DERs like energy storage systems (ESSs) on the demand side can be integrated into the proposed low-carbon DR program. Moreover, the DER aggregators can be introduced to better organize these demand-side DERs to provide operation flexibility for the power systems. Finally, alternative ambiguity sets can be further adapted to better handle the uncertainties.

NOMENCLATURE

I. Abbreviations

RES	Renewable energy source.
DG	Distributed generator.
FL	Flexible Load.
SO	Stochastic optimization.
CC	Chance-constrained.
RO	Robust optimization.
DRO	Distributionally robust optimization.
DRCC	Distributionally robust chance-constrained.

II. Indices and Sets

i	Index of the bus in the power system.
c	Index of the DRCC operation constraint.
t	Index of the time slot.
$\mathcal{N}^{\mathcal{B}}$	Set of the buses in the power system.
$\mathcal{C}$	Set of the DRCC operation constraints.
$\mathcal{T}$	Set of the time slots during the operation horizon.
$\mathbb{P}_{\boldsymbol{\xi}_t}$	Probability distribution of the total node power forecast error at time slot t.
$\mathbb{P}_{\boldsymbol{\xi}_t^{\mathrm{R}}}$	Probability distribution of the node RES power forecast error at time slot t.
$\mathbb{P}_{\boldsymbol{\xi}_t^{\mathrm{L}}}$	Probability distribution of the node Load power forecast error at time slot t.

III. Parameters

N^B	Number of the buses in the power system.
Δt	Operation time interval.
$\boldsymbol{\xi}_t$	Total node power forecast error at time slot t.
$\boldsymbol{\xi}_t^{\mathrm{R}}$	Node RES power forecast error at time slot t.
$\boldsymbol{\xi}_t^{\mathrm{L}}$	Node Load power forecast error at time slot t.
$\mathbf{C}_1^{\mathrm{G}}, \mathbf{C}_2^{\mathrm{G}}$	DG generation cost quadratic term and linear term coefficient matrices.
$\mathbf{C}^{\mathrm{R}}$	DG reserve cost coefficient matrix.
$\mathbf{C}^{\mathrm{R,cut}}, \mathbf{C}^{\mathrm{L,dis}}$	RES curtailment and Load discomfort compensation cost coefficient matrices.
π_t^{C}	Carbon trading price at time slot t.
δ	Carbon trading quantity interval.
λ, ρ	Carbon trading reward and penalty price coefficients.
$\mathbf{SF}^{\mathrm{G}}, \mathbf{SF}^{\mathrm{R}}, \mathbf{SF}^{\mathrm{L}}$	DG, RES, and Load power shift factor matrices.
$\mathbf{A}$	Node injection power shift factor matrix.
$\underline{\mathbf{P}}^{\mathrm{DG}}, \overline{\mathbf{P}}^{\mathrm{DG}}$	DG generation power lower bound and upper bound matrices.
$\overline{\mathbf{R}}^{\mathrm{U,DG}}, \overline{\mathbf{R}}^{\mathrm{D,DG}}$	DG upward reserve power and downward reserve power upper bound matrices.
$\overline{\mathbf{r}}^{\mathrm{U,DG}}, \overline{\mathbf{r}}^{\mathrm{D,DG}}$	DG upward ramping power and downward ramping power upper bound matrices.
$\mathbf{P}_t^{\mathrm{R,fore}}, \mathbf{P}_t^{\mathrm{L,fore}}$	Node RES forecast power and Load forecast power at time slot t.
$\Delta\underline{\mathbf{P}}_t^{\mathrm{L}}, \Delta\overline{\mathbf{P}}_t^{\mathrm{L}}$	Node DR adjustment power lower bound and upper bound matrices at time slot t.
$\overline{\mathbf{U}}^{\mathrm{L,dis}}$	Node Load maximum discomfort tolerance vector.
$\delta_t^{\mathrm{Sys,init}}$	System initial carbon emission quota coefficient at time slot t.
e_i^{G}	Carbon emission factor of the DG connected to bus i.
ε	Generic risk parameter.
$\varepsilon_{\mathrm{line}}, \varepsilon_{\mathrm{G,R}}, \varepsilon_{\mathrm{G,P}}$	System operation risk parameters.

IV. Variables

$\mathbf{P}_t^{\mathrm{G}}, \mathbf{R}_t^{\mathrm{G}}$	DG generation power and re-dispatch power vectors at time slot t.
$\mathbf{d}_t^{\mathrm{G}}$	DG re-dispatch participation coefficient vector at time slot t.
$\mathbf{R}_t^{\mathrm{U,G}}, \mathbf{R}_t^{\mathrm{D,G}}$	DG upward reserve power and downward reserve power vectors at time slot t.
$\mathbf{P}_t^{\mathrm{R,cut}}$	RES curtailment power vector at time slot t.
$\mathbf{P}_t^{\mathrm{FL}}, \Delta\mathbf{P}_t^{\mathrm{L}}$	Flexible Load power and DR adjustment power vectors at time slot t.
$E_t^{\mathrm{Sys,tr}}$	System carbon trading quantity at time slot t.
$\mathbf{P}_t^{\mathrm{inj}}, \mathbf{P}_t^{\mathrm{line}}$	Node injection power and transmission line power vectors at time slot t.
q_c, z_c	Auxiliary variables.

AUTHOR CONTRIBUTIONS

Ruifeng Zhao: Funding acquisition; project administration. **Zehao Song**: Conceptualization; data curation; formal analysis; investigation; methodology; resources; software; validation; visualization; writing—original draft; writing—review and editing. **Yinliang Xu**: Funding acquisition; project administration; supervision; writing—review and editing. **Jiangang Lu**: Funding acquisition; project administration. **Wenxin Guo**: Funding acquisition; project administration. **Haobin Li**: Funding acquisition; project administration.

ACKNOWLEDGEMENTS

This work was supported by the China Southern Power Grid Corporation Limited Project "Energy Management and Cluster Control Technology for Active Distribution Networks" (No. GDKJXM20222144). Ruifeng Zhao and Zehao Song are co-first authors.

CONFLICT OF INTEREST STATEMENT

The authors declare no conflicts of interest.

DATA AVAILABILITY STATEMENT

The data that support the findings of this study are available from the corresponding author upon reasonable request.

ORCID

Zehao Song https://orcid.org/0009-0004-0403-1610
Yinliang Xu https://orcid.org/0000-0001-5149-5101

REFERENCES

1. Guo, F., Ruijven, B.J.v., Zakeri, B., Zhang, S., Chen, X., Liu, C., et al.: Implications of intercontinental renewable electricity trade for energy systems and emissions. Nat. Energy 7(12), 1144–1156 (2022)
2. Fu, X., Zhang, C., Xu, Y., Zhang, Y., Sun, H.: Statistical machine learning for power flow analysis considering the influence of weather factors on photovoltaic power generation. IEEE Trans. Neural Networks Learn. Syst. (2024)
3. Heptonstall, P.J., Gross, R.J.: A systematic review of the costs and impacts of integrating variable renewables into power grids. Nat. Energy 6(1), 72–83 (2021)
4. Gao, H., Jiang, S., Li, Z., Wang, R., Liu, Y., Liu, J.: A two-stage multi-agent deep reinforcement learning method for urban distribution network reconfiguration considering switch contribution. IEEE Trans. Power Syst. (2024)
5. Fan, Q., Liu, D.: A wasserstein-distance-based distributionally robust chance constrained bidding model for virtual power plant considering electricity-carbon trading. IET Renewable Power Gener. 18(3), 545–557 (2024)
6. Fu, X., Wei, Z., Sun, H., Zhang, Y.: Agri-energy-environment synergy-based distributed energy planning in rural areas. IEEE Trans. Smart Grid (2024)
7. Song, Z., Xu, Y., Yang, L., Sun, H.: Carbon-aware peer-to-peer joint energy and reserve trading market for prosumers in distribution networks. IEEE Internet Things J. (2024)
8. Dadkhah, A., Vahidi, B., Shafie-khah, M., Catalão, J.P.: Power system flexibility improvement with a focus on demand response and wind power variability. IET Renewable Power Gener. 14(6), 1095–1103 (2020)
9. Morales-España, G., Martínez-Gordón, R., Sijm, J.: Classifying and modelling demand response in power systems. Energy 242, 122544 (2022)
10. Azarinfar, H., Khosravi, M., Ranjkeshan, R., Akbari, E.: Modelling of demand response programs in energy management of combined cooling, heat and power-based microgrids considering resiliency. IET Renewable Power Gener. 17(4), 964–981 (2023)
11. Jordehi, A.R.: Optimisation of demand response in electric power systems, a review. Renewable Sustainable Energy Rev. 103, 308–319 (2019)
12. Ding, G., Shu, Z., Xin, J., Lin, Z., Zhong, Z., Zhou, S., et al.: Research on optimal dispatch model of power grid considering the uncertainty of flexible resource demand response on the residential side. IET Renewable Power Gener. (2023)
13. Li, Y., Long, X., Li, Y., Ding, Y., Yang, T., Zeng, Z.: A demand–supply cooperative responding strategy in power system with high renewable energy penetration. IEEE Trans. Control Syst. Technol. 32(3), 874–890 (2024)
14. Dai, X., Wang, Y., Yang, S., Zhang, K.: IGDT-based economic dispatch considering the uncertainty of wind and demand response. IET Renewable Power Gener. 13(6), 856–866 (2019)
15. Levin, T., Bistline, J., Sioshansi, R., Cole, W.J., Kwon, J., Burger, S.P., et al.: Energy storage solutions to decarbonize electricity through enhanced capacity expansion modelling. Nat. Energy 8(11), 1199–1208 (2023)
16. Zakaria, A., Ismail, F.B., Lipu, M.H., Hannan, M.A.: Uncertainty models for stochastic optimization in renewable energy applications. Renew. Energy 145, 1543–1571 (2020)
17. Huang, C., Zhang, H., Song, Y., Wang, L., Ahmad, T., Luo, X.: Demand response for industrial micro-grid considering photovoltaic power uncertainty and battery operational cost. IEEE Trans. Smart Grid 12(4), 3043–3055 (2021)
18. Antoniadou-Plytaria, K., Steen, D., Tuan, L.A., Carlson, O., Mohandes, B., Ghazvini, M.A.F.: Scenario-based stochastic optimization for energy and flexibility dispatch of a microgrid. IEEE Trans. Smart Grid 13(5), 3328–3341 (2022)
19. Yang, X., Song, Z., Wen, J., Ding, L., Zhang, M., Wu, Q., et al.: Network-constrained transactive control for multi-microgrids-based distribution networks with soft open points. IEEE Trans. Sustainable Energy 14(3), 1769–1783 (2023)
20. Küçükyavuz, S., Jiang, R.: Chance-constrained optimization under limited distributional information: A review of reformulations based on sampling and distributional robustness. EURO J. Comput. Optim. 10, 100030 (2022)
21. Zhang, K., Xu, Y., Sun, H.: Joint chance-constrained program based electric vehicles optimal dispatching strategy considering drivers' response uncertainty. Appl. Energy 356, 122313 (2024)
22. Yang, Y., Wu, W., Wang, B., Li, M.: Chance-constrained economic dispatch considering curtailment strategy of renewable energy. IEEE Trans. Power Syst. 36(6), 5792–5802 (2021)
23. Conejo, A.J., Wu, X.: Robust optimization in power systems: a tutorial overview. Optim. Eng. 23(4), 2051–2073 (2022)
24. Park, B., Chen, Y., Olama, M., Kuruganti, T., Dong, J., Wang, X., et al.: Optimal demand response incorporating distribution lmp with pv generation uncertainty. IEEE Trans. Power Syst. 37(2), 982–995 (2022)
25. Qiu, Y., Li, Q., Huang, L., Sun, C., Wang, T., Chen, W.: Adaptive uncertainty sets-based two-stage robust optimisation for economic dispatch of microgrid with demand response. IET Renewable Power Gener. 14(18), 3608–3615 (2020)
26. Liu, H., Li, J., Zhang, S., Ge, S., Yang, B., Wang, C.: Distributionally robust co-optimization of the demand-side resources and soft open points allocation for the high penetration of renewable energy. IET Renewable Power Gener. 16(4), 713–725 (2022)
27. Li, J., Khodayar, M.E., Wang, J., Zhou, B.: Data-driven distributionally robust co-optimization of p2p energy trading and network operation for interconnected microgrids. IEEE Trans. Smart Grid 12(6), 5172–5184 (2021)
28. Coulson, J., Lygeros, J., Dörfler, F.: Distributionally robust chance constrained data-enabled predictive control. IEEE Trans. Autom. Control 67(7), 3289–3304 (2022)
29. Ding, Y., Morstyn, T., McCulloch, M.D.: Distributionally robust joint chance-constrained optimization for networked microgrids considering contingencies and renewable uncertainty. IEEE Trans. Smart Grid 13(3), 2467–2478 (2022)
30. Liao, W., Liu, D., Wu, Y., Liu, T.: Bi-level optimization of multi-regional power system considering low-carbon oriented synergy of both source and load sides. IET Renewable Power Gener. 18(3), 515–528 (2024)
31. Tan, Y., Shen, Y., Yu, X., Lu, X.: Low-carbon economic dispatch of the combined heat and power-virtual power plants: A improved deep reinforcement learning-based approach. IET Renewable Power Gener. 17(4), 982–1007 (2023)
32. Wang, Y., Wang, Y., Huang, Y., Yang, J., Ma, Y., Yu, H., et al.: Operation optimization of regional integrated energy system based on the modeling of electricity-thermal-natural gas network. Appl. Energy 251, 113410 (2019)
33. Jiang, Y., Ren, Z., Li, W.: Committed Carbon Emission Operation Region for Integrated Energy Systems: Concepts and Analyses. IEEE Trans. Sustainable Energy 15(2), 1194–1209 (2024)
34. Rayati, M., Bozorg, M., Cherkaoui, R., Carpita, M.: Distributionally robust chance constrained optimization for providing flexibility in an active distribution network. IEEE Trans. Smart Grid 13(4), 2920–2934 (2022)
35. Wang, R., Wen, X., Wang, X., Fu, Y., Zhang, Y.: Low carbon optimal operation of integrated energy system based on carbon capture technology, lca carbon emissions and ladder-type carbon trading. Appl. Energy 311, 118664 (2022)
36. Yang, L., Xu, Y., Gu, W., Sun, H.: Distributionally robust chance-constrained optimal power-gas flow under bidirectional interactions considering uncertain wind power. IEEE Trans. Smart Grid 12(2), 1722–1735 (2020)
37. Song, Z.: The topology and parameter data information of the IEEE 9-bus and 39-bus systems. Accessed 19 May 2024. https://github.com/szh16886596/Data-of-the-IEEE-9-Bus-System-and-IEEE-39-Bus-System
38. Economics, T.: Eu carbon permits. Accessed 27 March 2024. https://tradingeconomics.com/commodity/carborn

How to cite this article: Zhao, R., Song, Z., Xu, Y., Lu, J., Guo, W., Li, H.: Low-carbon demand response program for power systems considering uncertainty based on the data-driven distributionally robust chance constrained optimization. IET Renew. Power Gener. 1–13 (2024). https://doi.org/10.1049/rpg2.13021

APPENDIX A

The ambiguity set of the node load demand power forecast error is given as follows:

$$\mathcal{P}_t^{\mathrm{L}} := \{\mathbb{P}_{\xi_t^{\mathrm{L}}} : \mathbb{E}_{\mathbb{P}}[\boldsymbol{\xi}_t^{\mathrm{L}}] = \boldsymbol{\mu}_t^{\mathrm{L}}, \mathbb{E}_{\mathbb{P}}[(\boldsymbol{\xi}_t^{\mathrm{L}} - \boldsymbol{\mu}_t^{\mathrm{L}})(\boldsymbol{\xi}_t^{\mathrm{L}} - \boldsymbol{\mu}_t^{\mathrm{L}})^{\top}] = \boldsymbol{\Sigma}_t^{\mathrm{L}}\}, \tag{A1}$$

where $\boldsymbol{\xi}_t^{\mathrm{L}}$ is the node load demand power forecast error at time slot t, $\boldsymbol{\mu}_t^{\mathrm{L}}$ and $\boldsymbol{\Sigma}_t^{\mathrm{L}}$ are mean value vector and covariance matrix of $\boldsymbol{\xi}_t^{\mathrm{L}}$, respectively.

To take the uncertainty associated with loads in (7a) and (8), the ambiguity set of the total node power forecast error can be formulated as a compact form as follows:

$$\boldsymbol{\xi}_t = (\boldsymbol{\xi}_t^{\mathrm{R}} - \boldsymbol{\xi}_t^{\mathrm{L}}), \tag{A2a}$$

$$\mathcal{P}_t := \{\mathbb{P}_{\xi_t} : \mathbb{E}_{\mathbb{P}}[\boldsymbol{\xi}_t] = \boldsymbol{\mu}_t, \mathbb{E}_{\mathbb{P}}[(\boldsymbol{\xi}_t - \boldsymbol{\mu}_t)(\boldsymbol{\xi}_t - \boldsymbol{\mu}_t)^{\top}] = \boldsymbol{\Sigma}_t\}, \tag{A2b}$$

$$\boldsymbol{\mu}_t = \boldsymbol{\mu}_t^{\mathrm{R}} - \boldsymbol{\mu}_t^{\mathrm{L}}, \boldsymbol{\Sigma}_t = \boldsymbol{\Sigma}_t^{\mathrm{R}} - \boldsymbol{\Sigma}_t^{\mathrm{L}}. \tag{A2c}$$

In (A2), $\boldsymbol{\xi}_t$ is the total node power forecast error at time slot t, $\boldsymbol{\mu}_t$ and $\boldsymbol{\Sigma}_t$ are mean value vector and covariance matrix of $\boldsymbol{\xi}_t$, respectively.

Therefore, by considering $\boldsymbol{\xi}_t$, (7a) can be reformulated as follows:

$$\begin{aligned}\mathbf{P}_t^{\mathrm{inj}} = \mathbf{SF}^{\mathrm{G}}\left(\mathbf{P}_t^{\mathrm{G}} + \mathbf{R}_t^{\mathrm{G}}\right) + \mathbf{SF}^{\mathrm{R}}\left(\mathbf{P}_t^{\mathrm{R,fore}} - \mathbf{P}_t^{\mathrm{R,cut}}\right) \\ -\mathbf{SF}^{\mathrm{L}}\mathbf{P}_t^{\mathrm{FL}} + \boldsymbol{\xi}_t.\end{aligned} \tag{A3}$$

(8) can be reformulated as follows:

$$\inf_{\mathbb{P}_{\xi_t} \in \mathcal{P}_t} \xi_t \left\{ \underline{\mathbf{P}}^{\mathrm{line}} \le \mathbf{A} \cdot \mathbf{P}_t^{\mathrm{inj}} \le \overline{\mathbf{P}}^{\mathrm{line}} \right\} \ge 1 - \varepsilon_{\mathrm{line}}, \tag{A4a}$$

$$\inf_{\mathbb{P}_{\xi_t} \in \mathcal{P}_t} \xi_t \left\{ -_t^{\mathrm{D,G}} \le \mathbf{d}_t^{\mathrm{G}}\left(\mathbf{e}^{\top}\boldsymbol{\xi}_t\right) \le {}_t^{\mathrm{U,G}} \right\} \ge 1 - \varepsilon_{\mathrm{G,R}}, \tag{A4b}$$

$$\inf_{\mathbb{P}_{\xi_t} \in \mathcal{P}_t} \xi_t \left\{ \underline{\mathbf{P}}^{\mathrm{G}} \le \mathbf{P}_t^{\mathrm{G}} + \mathbf{d}_t^{\mathrm{G}}\left(\mathbf{e}^{\top}\boldsymbol{\xi}_t\right) \le \overline{\mathbf{P}}^{\mathrm{G}} \right\} \ge 1 - \varepsilon_{\mathrm{G,P}}. \tag{A4c}$$

Therefore, we can get the conclusion from (A1) to (A4) that the total node power forecast error $\boldsymbol{\xi}_t$ can be interpreted as the combination of the node RES power forecast error $\boldsymbol{\xi}_t^{\mathrm{R}}$ and the node load power forecast error $\boldsymbol{\xi}_t^{\mathrm{L}}$ regardless of the uncertainty distribution.